PCCP

PAPER

View Article Online
View Journal | View Issue

Check for updates

Cite this: *Phys. Chem. Chem. Phys.*, 2024, **26**, 23636

Metal–ligand delocalization of iron and cobalt porphyrin complexes in aqueous solutions probed by soft X-ray absorption spectroscopy†

Masanari Nagasaka, *[ab] Shota Tsuru [cd] and Yasuyuki Yamada [ef]

Received 24th May 2024,
Accepted 27th August 2024

DOI: 10.1039/d4cp02140a

rsc.li/pccp

Metal–ligand delocalization of metal porphyrin complexes in aqueous solutions was investigated by analyzing the electronic structure of both the metal and ligand sides using soft X-ray absorption spectroscopy (XAS) at the metal $L_{2,3}$-edges and nitrogen K-edge, respectively. In the N K-edge XAS spectra of the ligands, the energies of the C=N π* peaks of cobalt protoporphyrin IX (CoPPIX) are higher than iron protoporphyrin IX (FePPIX). The energy difference between the two lowest peaks in the XAS spectrum of CoPPIX is also larger than that of FePPIX. Nitrogen K-edge inner-shell calculations of metalloporphyrins with different central metals indicate that the energy differences between these peaks reflect the electronic configurations and spin multiplicities of metalloporphyrins. We also investigated the hydration structure of CoPPIX in aqueous solution by analyzing the electronic structure of the ligand and revealed that CoPPIX maintains its five-coordination geometry in aqueous solution. The present study shows high performance of N K-edge XAS of ligands for studying the coordination structures of metalloporphyrins in solutions rather than the metal $L_{2,3}$-edges of central metals.

Open Access Article. Published on 27 August 2024. Downloaded on 5/4/2026 4:07:56 PM.
This article is licensed under a Creative Commons Attribution-NonCommercial 3.0 Unported Licence.

Introduction

Porphyrin is known as a "pigment of life" because porphyrin and its metal complexes are widely utilized in various biochemical processes such as photosynthetic reactions, biological redox reactions, *etc.*[1] Moreover, metal complexes of porphyrins show unique catalytic activity for various chemical reactions and are well-recognized as important structural components of functional supramolecules.[2] Because the functions of metalloporphyrins are strongly dependent on the types, coordination structures, and electronic structures of central metal ions, many scientists have devoted a great deal of effort to reveal the relationship between the molecular structures of metalloporphyrins and their functions. Nonetheless, this process is often a bottleneck in research on metalloporphyrins.

If a crystalline solid of a metalloporphyrin is obtained, the detailed molecular structure can be determined by single-crystal X-ray structural analyses, allowing us to discuss the UV-Vis and EPR spectra based on their crystal structures.[3,4] Nevertheless, it is difficult to discuss the relationship between the functions of metalloporphyrins and their structures in solution or protein scaffolds with this method, because many metal porphyrin complexes function not in crystal phases but in solutions or protein scaffolds, where the structures of metalloporphyrins can be dynamically changed. For instance, regarding the active center of the heme protein, there are some examples of structural determination of the metal center based only on spectroscopic analyses, such as the determination of NO coordinating geometries based on changes in the hyperfine structures of EPR,[5] and the determination of coordination structures based on EXAFS experiments.[6] However, in many cases, it is necessary to investigate the relationship between the electronic structures of metalloporphyrins in solution or protein scaffolds and their coordination structures based on careful comparison of various types of spectral data, including UV-Vis, Mössbauer, EPR, NMR, and Raman spectroscopy, of model complexes whose structures are crystallographically determined.[6,7] Accordingly, analytical methods that enable direct comparison of the electronic structures of metalloporphyrins with their coordination structures in solution or protein scaffolds without using model complexes would become powerful tools for investigating metalloporphyrins.

[a] *Institute for Molecular Science, Myodaiji, Okazaki 444-8585, Japan. E-mail: nagasaka@ims.ac.jp*
[b] *Graduate Institute for Advanced Studies, SOKENDAI, Myodaiji, Okazaki 444-8585, Japan*
[c] *Lehrstuhl für Theoretische Chemie, Ruhr-Universität Bochum, D-44780 Bochum, Germany*
[d] *RIKEN Center for Computational Science, RIKEN, Kobe 650-0047, Japan*
[e] *Department of Chemistry, Graduate School of Science, Nagoya University, Nagoya 464-8602, Japan*
[f] *Research Center for Materials Science, Nagoya University, Nagoya 464-8602, Japan*
† Electronic supplementary information (ESI) available. See DOI: https://doi.org/10.1039/d4cp02140a

This journal is © the Owner Societies 2024

Open Access Article. Published on 27 August 2024. Downloaded on 5/4/2026 4:07:56 PM.
This article is licensed under a Creative Commons Attribution-NonCommercial 3.0 Unported Licence.

X-ray absorption spectroscopy (XAS) is an effective method for studying the electronic structures of metal porphyrin complexes with different elements. The electronic structures of the central metal ions have been extensively studied using XAS at the metal K-edges in the hard X-ray region. In the Fe K-edge XAS spectra of the Fe complexes, the electronic and spin states of the Fe centers are reflected in the transition peaks of the Fe 1s core electrons to the Fe 4p unoccupied orbitals caused by mixing of the Fe 4p and Fe 3d orbitals.[8,9] The structures of oxyhemoglobin in solution were investigated using Fe K-edge XAS.[10] The relaxation processes from high-spin states to ground states after photoexcitation to MLCT states were investigated by time-resolved hard X-ray XAS, selecting the absorption edges of the central metal ions with a time scale of several hundred picoseconds.[11–13] The catalytic reactions involving metalloporphyrins were investigated by hard X-ray XAS.[14,15] Despite such effort, thorough understanding of metal–ligand delocalization in metalloporphyrins has yet to be achieved, mainly because hard X-ray XAS only observes central metal ions and does not directly observe ligands.

The soft X-ray region below 2 keV includes the K-edges of C, N, O, and F, as well as the $L_{2,3}$-edges of transition metals such as Mn, Fe, Co, Ni, and Cu.[16] The Fe $L_{2,3}$-edge XAS spectra exhibit the transition of the Fe 2p core electrons to the Fe 3d unoccupied orbitals and observed the delocalization between the 3d orbitals of the Fe centers and the 2p orbitals of the ligands. The electronic structures of iron protoporphyrin IX (FePPIX) in solution were studied by Fe $L_{2,3}$-edge XAS in fluorescence yield,[17,18] and those of cobalt protoporphyrin IX (CoPPIX) were studied by Co $L_{2,3}$-edge XAS.[19] The coordination of solvent molecules to iron porphyrins were investigated by Fe $L_{2,3}$-edge XAS.[20] The metal–ligand delocalization in metal complexes was investigated by electronic structural analyses of ligands employing C and N K-edge XAS.[21–27] The central metal dependence of metal–ligand delocalization was investigated by N K-edge XAS measurements of solid metallo-octaethylporphyrins in a series of 3d metal ions.[28] The electronic structures of solid Zn porphyrin systems were investigated by the N K-edge XAS experiment with the theoretical calculations using time-dependent density functional theory (TDDFT).[29] The photoexcitation dynamics of metal complexes in solution have been investigated using time-resolved XAS in the soft X-ray region.[23,26,30–32]

As discussed in Section S1 of the ESI,† the XAS spectra of metalloporphyrins were mainly measured using fluorescence yield, but the spectral shapes deviated from the true absorption spectra due to the self-absorption effect of fluorescence light. Meanwhile, flat microjets with a thickness of several micrometers were used to measure the XAS spectra in transmission mode.[23,26,27,33] However, XAS measurements of flat microjets cannot be applied to all liquid samples because of the restrictions of vapor pressures. To overcome these difficulties, we developed an XAS measurement method using a liquid cell, in which the thickness of a liquid layer is controllable from 20 nm to 40 μm.[34,35] There is no limit to sample selection for XAS measurements using liquid cells because liquid samples are exchangeable using a syringe pump.

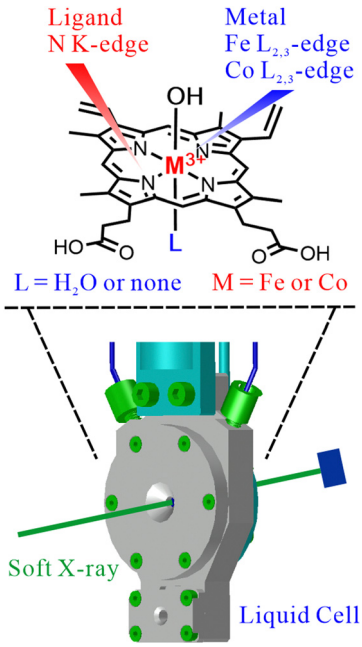

Fig. 1 A schematic of the liquid cell for XAS of metalloporphyrins in aqueous solutions. XAS spectra of central metals in metalloporphyrins were obtained at the Fe or Co $L_{2,3}$-edge and those of ligands were obtained at the N K-edge, respectively. The hydration of the metalloporphyrin was also investigated by the N K-edge XAS.

In this study, we have investigated the metal–ligand delocalization of FePPIX and CoPPIX in aqueous solutions based on electronic structural analyses of both the metal ion and ligand sides employing XAS at the metal $L_{2,3}$-edges and the N K-edge, respectively, by utilizing our liquid cell apparatus, as shown in Fig. 1. The electronic configuration and spin multiplicity of the metal complexes were directly observed by N K-edge XAS of the ligands to determine the dependence on the central metal ions. For the comparison of the metal complexes, we also measured N K-edge XAS spectrum of protoporphyrin IX (PPIX), which consists of the same porphyrin ring with no central metal ion. The hydration of CoPPIX in aqueous solution has also been discussed based on electronic structural analysis of the ligand. It is important to determine the hydrated or coordinated structures of metalloporphyrins in solution or protein scaffolds because many metal porphyrin complexes function not in crystal phases but in solutions or protein scaffolds, where these structures are dynamically changed with the connection of solvated molecules.

Methods

Sample preparation

Samples of FePPIX, CoPPIX, and PPIX were purchased from Sigma Aldrich and were used without further purifications. Aqueous solution of NaOH (0.5 M) was purchased from Wako Chemicals. Solutions of FePPIX, CoPPIX, and PPIX with the concentration of 50 mM were prepared by dissolving these complexes in 0.5 M NaOH aqueous solutions.

Open Access Article. Published on 27 August 2024. Downloaded on 5/4/2026 4:07:56 PM. This article is licensed under a Creative Commons Attribution-NonCommercial 3.0 Unported Licence.

Soft X-ray absorption spectroscopy

The XAS experiments were performed at the soft X-ray undulator beamline BL3U at the UVSOR-III Synchrotron.[36] The detail of the transmission-type liquid cell for XAS of liquid samples was described previously.[34,35] The liquid cell was in an ambient pressure of helium gas, where a liquid layer was sandwiched between two 100 nm thick SiC membranes. For appropriate absorbance of soft X-rays, the thickness of the liquid layer was controlled from 20 nm to 40 μm by adjusting the helium pressure around the liquid cell: the liquid layer becomes thinner by increasing the helium pressure, and *vice versa*. There is no limit to sample selection because liquid samples were introduced to the liquid cell by using a syringe pump. The required exchange amount of liquid sample is less than 1 mL owing to the reduced volume of the liquid cell. The sample temperature was kept at 25 °C by using a chiller system.

In the present system, Fe and Co $L_{2,3}$-edge XAS spectra can detect several mM central metal ions of metalloporphyrins in both aqueous solutions and organic solvents. Several mM ligands in aqueous solutions can be observed in C and N K-edge XAS. In organic solvents, the detection limit of ligands depends on both the sorts of solute and solvent molecules. The C K-edge XAS can detect the C=N π* peaks of ligands in organic solvents which consist of single bonds such as methanol, ethanol, tetrahydrofuran, *etc.* These details are described in Section S2 of the ESI.† The XAS spectra were obtained using the Beer–Lambert law, $\ln(I_0/I)$, where I_0 and I were the transmission signals of pure solvent, which was 0.5 M NaOH aqueous solutions and 50 mM complexes dissolved in 0.5 M NaOH aqueous solutions, respectively. The samples were flown with 50–100 μL hour^{-1} during the measurements. The beam size was 200 μm × 200 μm, and the photon densities at the N K-edge, the Fe $L_{2,3}$-edge, and the Co $L_{2,3}$-edge were 1×10^{16}, 5×10^{15}, and 2×10^{15} photons m^{-2} s^{-1}, respectively. The XAS spectra were obtained by collecting the photon fluxes with scanning the photon energies, where the photon fluxes at each photon energy were collected using a photodiode detector with the dwell time of 2 s. The XAS spectra of same samples were cyclically measured with several times for checking the radiation induced sample damages. The energy resolutions of the incident soft X-rays were 0.7 eV at the Fe $L_{2,3}$-edge, 0.78 eV at the Co $L_{2,3}$-edge, and 0.2 eV at the N K-edge, respectively. The photon energies were precisely calibrated by measuring XAS of the polymer film before and after the sample measurements.[37] Thus, the energy resolution did not affect the energetic positions of the XAS peaks.

Inner-shell calculation

Geometries of FePPIX, CoPPIX, and PPIX were optimized using DFT with the PBE0 exchange–correlation functional, which was sufficiently accurate to describe the structures of transition metal complexes.[38] The optimized geometries are shown in Section S9 of the ESI.† The inner-shell calculations were performed with TDDFT applying the Tamm–Dancoff approximation (TDA) in conjunction with the CAM-B3LYP functional.[39] For the ground state of FePPIX (open-shell system), unrestricted DFT (UDFT) was utilized otherwise specified. The inner-shell spectra were broadened by 0.7 eV with a Gaussian line shape and shifted by +11.93 eV. The constant energy shift is a systematic error of TDDFT, attributable to relaxation of the electrons caused by the core–hole and by self-interaction errors and was determined as the value needed to align the calculated spectrum of PPIX with the corresponding experimental one. The def2-TZVPP basis set was used for all the geometry optimizations and the spectral simulations otherwise specified. Calculations were conducted using Q-Chem 5.4.2[40] and NTChem 2013 v13.1.0.[41] It might be noteworthy that the present inner-shell calculations are based on the method summarized in the reviews,[42,43] which does not rely on the symmetry of systems.

Spin multiplicity of each system was specified by the numbers of the spin-up and spin-down electrons, where FePPIX in the calculation had 172 spin-up and 167 spin-down electrons, respectively, whereas both the numbers of the electrons were 170 for CoPPIX. The visualized Kohn–Sham (KS) orbitals of each system confirmed that the open shells were localized on the central metal ion. Although the ground-state ansatz as the reference of TDDFT calculated with UDFT for an open-shell system may generally suffer from spin contamination, the expectation value of the spin angular momentum obtained for FePPIX, $\langle S^2 \rangle$ = 8.85, confirmed that the ansatz was almost of the pure spin sextet (high spin) state, where the value must be 8.75.

Results and discussion

XAS experiments of metal porphyrin complexes

Fig. 2 shows the Fe $L_{2,3}$-edge XAS spectrum of FePPIX and the Co $L_{2,3}$-edge XAS spectrum of CoPPIX in aqueous solutions. As shown in the inset of Fig. 2, hydroxo complexes of FePPIX and CoPPIX were formed in condensed OH^- aqueous solutions, where the axial ligands of Cl^- ions are exchanged to OH^- ions. As discussed in Section S3 of the ESI,† the previous studies indicated that FePPIX forms a cofacial dimer, where two five-coordinated FePPIX are stacked, in this condition.[18,44] Golnak *et al.* observed no large spectral difference between XAS of FePPIX monomer and dimers.[18,22]

Since the metal $L_{2,3}$-edge XAS spectra correspond to the transition of metal 2p electron to unoccupied 3d orbitals, which can be split to the ligand field, we determined the energetic positions of three peaks in the lowest energy region of the metal L_3-edge XAS spectra by the fitting procedure; the lowest, second-lowest, and third-lowest peaks were named the first, second, and main peaks, respectively. The energetic positions of these peaks in FePPIX and CoPPIX are shown in Section S4 of the ESI.† In the Fe L_3-edge XAS spectrum of FePPIX, the energy shifts of the first and second peaks from the main peak are −2.395 and −1.323 eV, respectively. The energy shifts of the first and second peaks from the main peak in the CoPPIX spectrum are −3.268 and −1.562 eV, respectively. The energy

 This journal is © the Owner Societies 2024

Open Access Article. Published on 27 August 2024. Downloaded on 5/4/2026 4:07:56 PM.
This article is licensed under a Creative Commons Attribution-NonCommercial 3.0 Unported Licence.

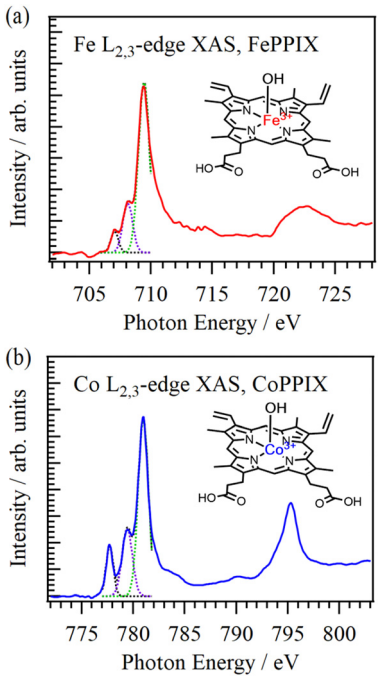

Fig. 2 Metal $L_{2,3}$-edge XAS spectra of central metals in aqueous solution. (a) Fe $L_{2,3}$-edge XAS spectrum of FePPIX in aqueous solution. (b) Co $L_{2,3}$-edge XAS spectrum of CoPPIX in aqueous solution. Three peaks in the L_3-edges obtained by the fitting procedure are also shown. The insets show molecular structures of FePPIX and CoPPIX.

differences of the multiple peaks in the CoPPIX spectrum are larger than those of FePPIX. Therefore, the XAS spectrum of CoPPIX shows sharper spectral shapes, where different peaks are clearly separated from each other, compared to that of FePPIX.

The N K-edge XAS spectra of the ligands in the metal complexes enable us to discuss the central metal dependence of metal–ligand delocalization in the same photon energy regions. Fig. 3 shows the N K-edge XAS spectra of 50 mM FePPIX, CoPPIX, and PPIX. The structures around N atoms in ligands are close to those of pyridine molecules (C–N═C), which consist of the single and double bonds of the N atom with the C atoms or the C═N double bond spreads equivalently to both sides of the C atoms. We simply call these structures C═N parts, hereafter. Since PPIX has no central metal ion, the ligand shows two different types of C═N parts, whether the H atoms are connected or not: one is the C–N═C bond which is same as FePPIX and CoPPIX, and the other is close to the structures of pyrrole molecules (C–(NH)–C). Thus, the N K-edge XAS spectrum of PPIX consists of two C═N π* peaks, where the energetic positions of the first and second peaks are 397.760 and 399.929 eV, respectively. The energetic positions of these peaks in the N K-edge XAS spectra are shown in Section S5 of the ESI.† The energy difference between the first and second peaks in the PPIX spectrum is 2.169 eV.

In contrast to PPIX, the C═N groups of the ligands in FePPIX and CoPPIX are equivalent because of the coordination of Fe and Co ions in these metal complexes. The N K-edge XAS

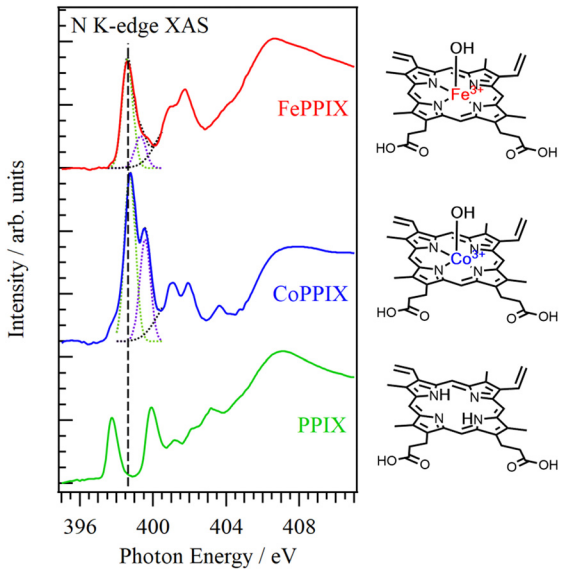

Fig. 3 Nitrogen K-edge XAS spectra of FePPIX, CoPPIX, and PPIX in aqueous solutions. The C═N π* peaks of ligands are fitted by those of different unoccupied orbitals. Dashed line indicates the energetic position of the first peak in the FePPIX spectrum. The inset shows the molecular structures of FePPIX, CoPPIX, and PPIX.

spectra of FePPIX and CoPPIX show two C═N π* peaks derived from the delocalization of the metal 3d orbitals to the ligand 2p orbitals. Note that a shoulder on the lower photon energy side of the first peak is observed in the spectrum of CoPPIX. The first peak in the spectrum of FePPIX is 0.832 eV higher than that of PPIX and is located between the first and second peaks in the spectrum of PPIX. The first peak in the CoPPIX spectrum is 0.139 eV higher than that of FePPIX. The energy differences between the first and second peaks in the FePPIX and CoPPIX spectra are 0.710 and 0.828 eV, respectively. The energy difference between the multiple peaks in the spectrum of CoPPIX is larger than that of FePPIX. This tendency is consistent with the results of the metal L_3-edge XAS shown in Fig. 2.

Nitrogen K-edge inner-shell calculations

Fig. 4 shows the calculated C═N π* peaks of the ligands in the N K-edge inner-shell spectra of FePPIX, CoPPIX, and PPIX. Although the axial ligands of both FePPIX and CoPPIX complexes are replaced from Cl^- into OH^- ions in the actual aqueous solutions, the axial ligands were not changed in the inner-shell calculations. It is because the spectra computed for the complexes having Cl^- as the counter anion rather seem close to those obtained in the experiment, possibly because geometry optimization with the OH^- ion neglecting the solvent effects overestimates covalency between the central metal ion and OH^-, *i.e.* the Co–O bond distance for Co–(OH^-) is 1.80 Å while that for Co–(H_2O) is 2.07 Å despite fluctuation and replacement of OH^- caused by the bulk H_2O molecules. Possible causes of the errors as well as observed mismatch of the peak intensities in the simulated spectra, are discussed in Section S6 of the ESI.† Despite the observed mismatch of the peak intensities, it may still make sense to interpret the

Open Access Article. Published on 27 August 2024. Downloaded on 5/4/2026 4:07:56 PM.
This article is licensed under a Creative Commons Attribution-NonCommercial 3.0 Unported Licence.

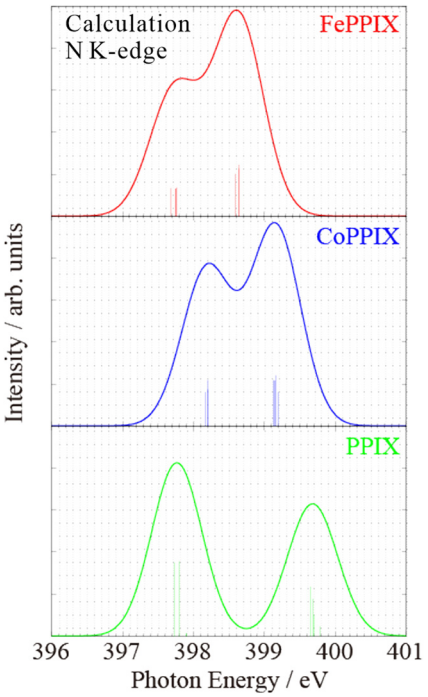

Fig. 4 Calculated C═N π* peaks of ligands in the N K-edge inner-shell spectra of FePPIX, CoPPIX, and PPIX.

difference between the N K-edge inner-shell spectra measured for FePPIX and CoPPIX based on that between the computed spectra, because the effects neglected in the inner-shell calculations are common to FePPIX and CoPPIX.

The calculated N K-edge inner-shell spectrum of PPIX shows two C═N π* peaks in the energetic positions of 397.76 and 399.68 eV. The calculated energetic positions of the C═N π* peaks as well as the occupied and virtual orbitals between which electronic transition takes place in each excitation are shown in Section S5 of the ESI.† As discussed in the XAS experiments, two C═N π* peaks are derived from the different types of C═N parts, whether the H atoms connect or not. The energy difference of the second peak from the first peak in the calculated spectrum of PPIX is 1.92 eV and consistent with the experimental value (2.169 eV) with reasonable accuracy.

The calculated inner-shell spectrum of FePPIX shows two C═N π* peaks, whose energetic positions are 397.75 and 398.63 eV. The two C═N π* peaks are derived from the delocalization of the metal 3d orbitals to the ligand 2p orbitals. The intensity of the first peak is lower than that of the second peak in the simulated inner-shell spectrum, which is contrary to that obtained in the XAS experiment. Although the first peak in the calculated spectrum of FePPIX (397.75 eV) is close to that of PPIX (397.76 eV), the C═N π* peaks of FePPIX are mainly located between the first and second peaks of PPIX. The energy difference between the second and first peaks in the calculated spectrum of FePPIX is 0.88 eV. The inner-shell spectrum of CoPPIX shows two C═N π* peaks at the energetic positions of 398.19 and 399.17 eV. The energy difference between the second and first peaks in the calculated spectrum of CoPPIX (0.98 eV) is found to be larger than that of FePPIX (0.88 eV). The first peak in the calculated spectrum of CoPPIX shows a higher energy shift by 0.44 eV than that of FePPIX. These computational results are qualitatively consistent with the experimental results.

Interpretation of metal–ligand delocalization

With appropriate selection of the exchange–correlation functional, the KS orbitals obtained in DFT calculations can be considered as molecular orbitals reflecting the dynamical electronic correlation. Moreover, TDDFT with TDA can be regarded as configuration interaction singles (CIS) utilizing the KS orbitals. Therefore, electron excitations described by TDDFT can be interpreted as electron transitions from occupied KS orbitals to virtual KS orbitals. Taking advantage of these features of (TD)DFT, we interpreted the N K-edge inner-shell spectra based on molecular orbital pictures.

We emphasize that odd number of the electrons like the case of FePPIX or spin multiplicity where $\langle S_z \rangle \neq 0$ complicates such interpretation. As mentioned above, the UDFT ansätze may suffer from spin contamination and the orbital energies differ for the spin-up and spin-down electrons occupying the KS orbitals with a same character. For example, UDFT gives $\langle S^2 \rangle$ = 1.60 for FePPIX with 170 spin-up electrons and 169 spin-down electrons, whereas the $\langle S^2 \rangle$ value must be 0.75 for the pure spin doublet (low spin) state. Meanwhile, restricted open-shell DFT (RODFT), where the ansätze are spin eigenfunctions and the orbital energies are common to the spin-up and spin-down electrons, is problematic for TDDFT, because the Fock matrices are not fully diagonalized. Considering these factors, we conducted RODFT calculations to discuss the SCF and orbital energies with respect to the spin multiplicity. Results of the RODFT calculations are shown in Section S7 of the ESI.† For discussing the effects of spin multiplicity on the inner-shell spectra, we conducted RODFT calculations for cations in the manner of the equivalent core or $(Z + 1)$ approximation,[45] instead of direct inner-shell calculations, and show the results in Section S8 of the ESI.†

As shown in Fig. 5(a), in metalloporphyrins, the 3d electronic orbitals of the central metals are delocalized with the 2p electronic orbitals of the ligands. Therefore, the energy shifts of the C═N π* peaks in the N K-edge XAS spectra of the ligands can be explained by the ligand-field theory of metal complexes. Fig. 5(b) shows the 3d electronic configuration of FePPIX and CoPPIX under the ligand-field effect. Although Fe(III) porphyrin exhibits a $3d_5$ electronic configuration and its spin configuration can be low, high, or intermediate depending on the types of axial ligand, FePPIX with the axial ligands of Cl^- or OH^- ions tends to lie in the high-spin state because the coordination of Cl^- or OH^- ions generally results in relatively small crystal-field stabilization energies.[3] The exchange interaction also stabilizes the electronic state, where all the 3d orbitals are occupied by one electron each in a $3d_5$ electronic configuration. It is known from Mössbauer spectroscopy that FePPIX has the highest spin multiplicity and maintains a five-coordination geometry in solution.[46]

 This journal is © the Owner Societies 2024

Open Access Article. Published on 27 August 2024. Downloaded on 5/4/2026 4:07:56 PM.
This article is licensed under a Creative Commons Attribution-NonCommercial 3.0 Unported Licence.

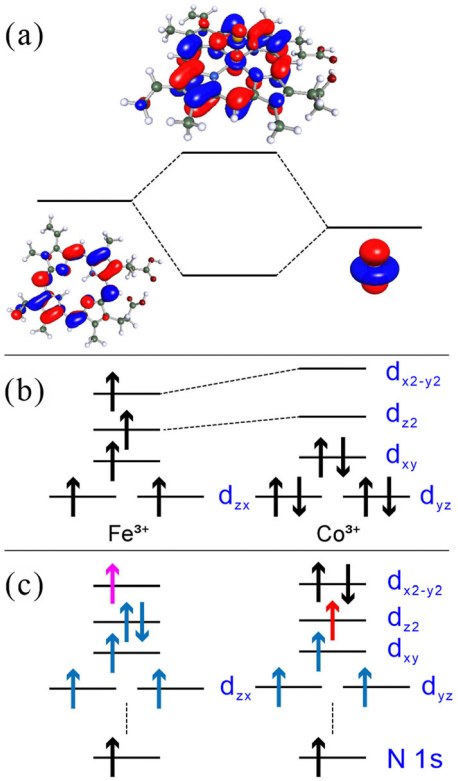

Fig. 5 Schematic electronic configurations for the interpretation of metal–ligand delocalization. (a) Schematic diagram of an orbital made from a 3d orbital of a central metal ion and a π* orbital of PPIX. (b) Schematic 3d electronic configuration of the Fe^{3+} and Co^{3+} ions under the ligand-field effect. (c) Schematic 3d electronic configurations of FePPIX after the first and second lowest-energy N 1s core excitations in left and right panels, respectively. The electrons depicted with magenta and red arrows feel Coulomb potentials from the nuclei screened by five and three electrons indicated by blue arrows in the 3d configurations, respectively.

CoPPIX exhibits a $3d_6$ electronic configuration. Because the $3d_6$ electronic configuration includes at least one electron pair, the stabilization effect of the exchange interaction in the $3d_6$ electronic configuration is smaller than that in the high-spin $3d_5$ electronic configuration, as estimated by the RODFT calculations summarized in Section S7 of the ESI.† Consequently, CoPPIX has the lowest spin multiplicity, where the electron pairs occupy the d_{zx}, d_{yz}, and d_{xy} orbitals, as confirmed by Co $L_{2,3}$-edge XAS of CoPPIX.[19] Note that the spin multiplicity of each transition metal complex is determined by the crystal field splitting energy and the pairing energy. Considering the high-spin state of FePPIX is more stable than the low-spin state only by 0.34 eV, FePPIX may also take the low-spin state once the Cl^- or OH^- ligand has been replaced with a strong field ligand such as NH_3. The energy diagram of CoPPIX indicates that the energetic positions of the two C═N π* peaks in the N K-edge XAS spectra of the ligands are associated with the d_{z^2} and $d_{x^2-y^2}$ orbitals. The unoccupied orbitals, such as d_{z^2} and $d_{x^2-y^2}$ observed in XAS are stabilized by the induced polarization of the effective nuclear charge increase after the excitation of the N 1s core electrons, which causes a lower energy shift of the XAS peaks.[47] The induced polarization of the unoccupied orbitals decreases by increasing the number of occupied electrons beneath these unoccupied orbitals, resulting in higher energetic positions of the corresponding XAS peaks. FePPIX has only three electrons in the 3d orbitals beneath the d_{z^2} and $d_{x^2-y^2}$ orbitals, whereas CoPPIX has six electrons in these electronic orbitals. Therefore, the C═N π* peaks in the spectrum of CoPPIX show higher energy shifts than those of FePPIX. The shoulder of the first C═N π* peak in the spectrum of CoPPIX was not reproduced in the present inner-shell calculations. It is possible that the molecular structure of CoPPIX was distorted by the interactions with solvent molecules, and the shoulder on the lower energy side emerged due to the delocalization of the N 2p orbitals with the Co $3d_{zx}$, $3d_{yz}$, and $3d_{xy}$ orbitals. Further study is required for confirming the assignment of the shoulder in the spectrum of CoPPIX.

The energy differences between the two C═N π* peaks in the N K-edge XAS spectra of FePPIX and CoPPIX can also be explained by the induced polarization effect. In the CoPPIX spectrum, the induced polarization effect is not affected by the excitation of the N 1s core electrons to either the d_{z^2} or $d_{x^2-y^2}$ orbital because the configuration of the occupied electrons beneath these electronic orbitals is common in the two excitation channels. As shown in Fig. 5(c), the two C═N π* peaks corresponding to the d_{z^2} and $d_{x^2-y^2}$ orbitals in the FePPIX spectrum exhibit different induced polarization effects. The first peak is associated with the transition of the N 1s core electrons to the d_{z^2} orbital, and the second peak is associated with that of the $d_{x^2-y^2}$ orbital. Because the induced polarization decreases as the number of occupied electrons in the inner-shells increases, the induced polarization effect is weaker for the electronic configuration shown in the left panel of Fig. 5(c) than that for the electronic configuration shown in the right panel. As a result, the higher energy shift effect of the first peak caused by the weaker induced polarization is stronger than that of the second peak, resulting in a smaller energy difference between the two C═N π* peaks in the spectrum of FePPIX than in that of CoPPIX. These energy diagrams also explain the energy differences between the multiple peaks in the metal L_3-edge XAS spectra of FePPIX and CoPPIX.

As described above, ligand-field splitting in metal complexes can be observed in the C═N π* peaks of ligands in the N K-edge XAS spectra. In contrast to the metal $L_{2,3}$-edge XAS spectra, which cannot directly compare the electronic structures of different central metal ions, the N K-edge XAS measurements enable us to observe the central metal dependence of the metal–ligand delocalization by electronic structural analyses of the ligands. The different energy shifts of the C═N π* peaks in the N K-edge XAS spectra of FePPIX and CoPPIX can be explained by the induced polarization effect of the core electrons in the metal 3d electronic configurations.

Consideration of the hydration of CoPPIX

It is known for decades that FePPIX in aqueous solution maintains a five-coordinate geometry with the highest spin multiplicity.[46] Meanwhile, the coordination geometry of

Open Access Article. Published on 27 August 2024. Downloaded on 5/4/2026 4:07:56 PM.
This article is licensed under a Creative Commons Attribution-NonCommercial 3.0 Unported Licence.

CoPPIX in aqueous solution was not identified yet. Although the previous Co $L_{2,3}$-edge inner-shell calculation indicated the lowest spin multiplicity of CoPPIX in aqueous solution, the hydrated structure could not be determined, because the spectral shape of the inner-shell spectrum calculated for CoPPIX with five-coordination geometry did not change from that of the spectrum calculated for octahedral CoPPIX with a hydrated water molecule.[19]

To investigate whether CoPPIX in an aqueous solution forms a hydrated octahedral structure, we calculated the N K-edge inner-shell spectrum of octahedral CoPPIX with an additionally coordinated water molecule, as well as that of planar CoPPIX without counter anion, as shown in Fig. 6. The spectrum of octahedral CoPPIX shows only one C=N π* peak around 398.8 eV. This is different from the spectrum of CoPPIX with a five-coordination geometry, which consists of two C=N π* peaks, as shown in Fig. 4. The $d_{x^2-y^2}$ and d_{z^2} orbitals are degenerated in the octahedral CoPPIX, resulting in a single C=N π* peak in the N K-edge inner-shell spectrum. Meanwhile, the spectrum of planar CoPPIX shows the first C=N π* peak around 396.5 eV, which is too low compared to the experimental one (398.731 eV), reflecting the low-lying d_{z^2} orbital due to the absence of the metal–ligand repulsion in the *z*-direction.

The N K-edge XAS spectrum of CoPPIX in aqueous solution shows two C=N π* peaks separated by 0.828 eV (Fig. 3), proposing that the CoPPIX complex does not form an octahedral structure and maintains its five-coordination geometry in aqueous solution. Because both FePPIX and CoPPIX maintain a five-coordination geometry in aqueous solution, the energy shift of the C=N π* peak of CoPPIX from that of FePPIX shows a same tendency with the result of solid metallo-octaethylporphyrins.[28] Note that the spectral changes of N K-edge XAS would be considered regarding the ligand-field theory when the hydration structures of metalloporphyrins are changed with different metal ions in solution. From the electronic structural analyses of the ligands employing N K-edge XAS, we have clarified the coordination structures of metalloporphyrins in aqueous solutions. This method is generally effective because it analyzes the coordination structures in solutions not at the central metal side but at the ligand side in metal complexes.

Conclusions

The metal–ligand delocalization of FePPIX and CoPPIX in aqueous solutions was investigated by electronic structural

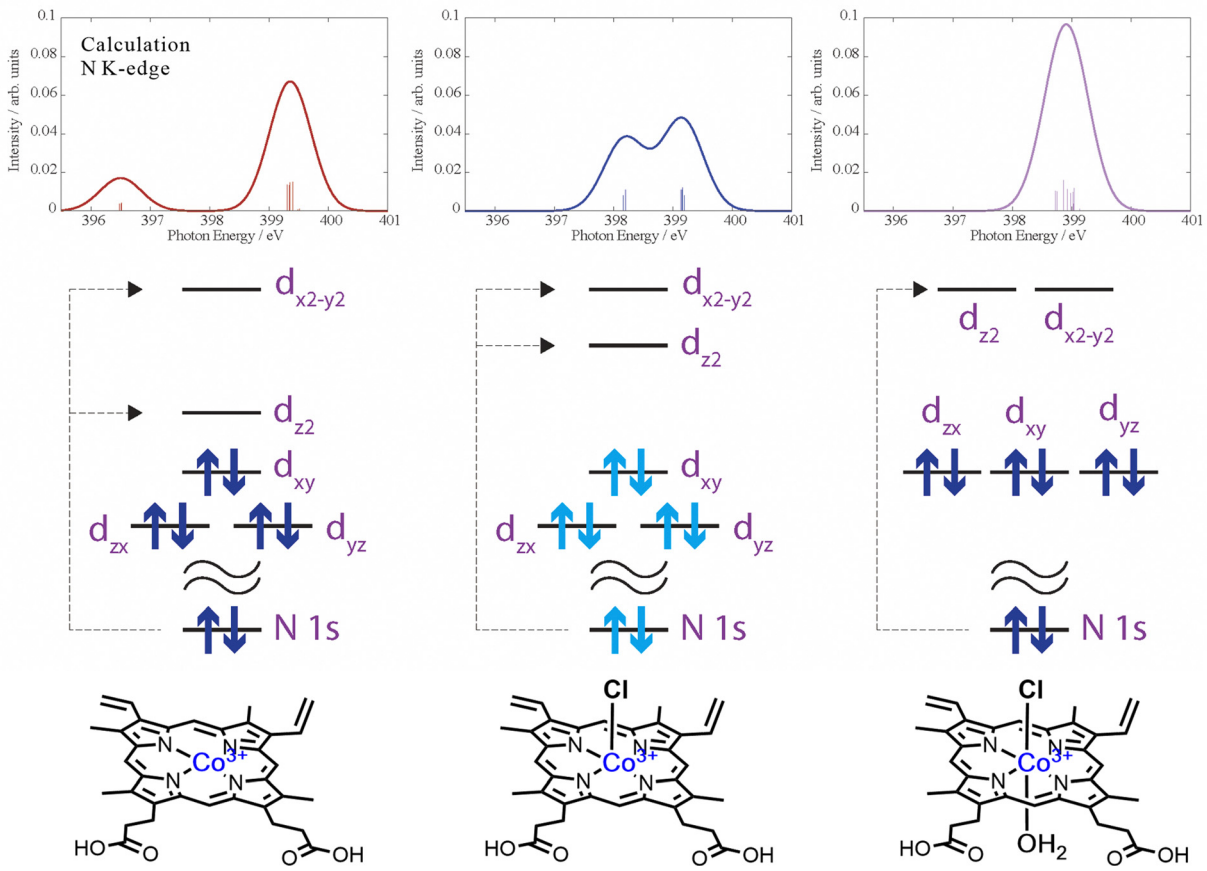

Fig. 6 Calculated C=N π* peaks in the N K-edge inner-shell spectra of planar CoPPIX without counter anion, five-coordinate CoPPIX, and octahedral CoPPIX with a hydrated water molecule. These molecular structures are shown at the bottom. The orbital diagrams schematically show the split of the 3d orbitals of the Co^{3+} cation and the electron configuration of each coordination. Dashed arrows of each diagram indicate the core excitations corresponding to the first and second peaks in each N K-edge inner-shell spectrum.

 This journal is © the Owner Societies 2024

Open Access Article. Published on 27 August 2024. Downloaded on 5/4/2026 4:07:56 PM.
This article is licensed under a Creative Commons Attribution-NonCommercial 3.0 Unported Licence.

analyses of both the metal and ligand sides, employing XAS at the metal $L_{2,3}$-edges and the N K-edges, respectively. In the metal L_3-edge XAS spectra, multiple peaks are observed owing to ligand-field splitting of the metal 3d orbitals. The energy difference between the multiple peaks in the L_3-edge spectrum of CoPPIX is larger than that of FePPIX. The N K-edge XAS spectrum of PPIX consists of two C═N π* peaks, which are derived from the different types of C═N parts, whether the H atoms connect or not. The N K-edge XAS spectra of FePPIX and CoPPIX show two C═N π* peaks derived from delocalization of the metal 3d orbitals to the ligand 2p orbitals. The first peak in the N K-edge XAS spectrum of CoPPIX shows a higher energetic position than that of FePPIX. The energy difference between the multiple peaks in the CoPPIX spectrum is larger than that of FePPIX, which is consistent with the results of the metal L_3-edge XAS spectra.

Nitrogen K-edge inner-shell calculations of the ligands qualitatively reproduced the energy shifts of the C═N π* peaks in the spectra of PPIX, FePPIX, and CoPPIX. These energy shifts can be explained by the ligand-field theory for metal complexes. FePPIX has a $3d_5$ electronic configuration with the highest spin multiplicity, where all 3d orbitals are half-occupied.[46] CoPPIX has a $3d_6$ electronic configuration with the lowest spin multiplicity, in which electron pairs occupy the d_{zx}, d_{yz}, and d_{xy} orbitals. The two C═N π* peaks in the N K-edge XAS spectra of the ligands are associated with the d_{z^2} and $d_{x^2-y^2}$ orbitals. The XAS peaks show higher-energy shifts with a decrease in the induced polarization of the N 1s core hole when the number of occupied electrons beneath the corresponding unoccupied orbitals increased. This induced polarization effect explains the higher energy shift of the C═N π* peak and the larger energy difference between the multiple peaks in the spectrum of CoPPIX compared to those of FePPIX.

Because the Co $L_{2,3}$-edge inner-shell spectrum of CoPPIX with a five-coordination geometry does not differ from that of octahedral CoPPIX with an additional coordinating water molecule,[19] the Co $L_{2,3}$-edge XAS measurement does not determine the hydration structure of CoPPIX in aqueous solution. Based on the number of C═N π* peaks and the distance between them in the calculated N K-edge inner-shell spectra of CoPPIX, we have found that the CoPPIX complex does not form an octahedral structure and maintains a five-coordination geometry in aqueous solutions.

In this study, we have revealed that the metal–ligand delocalization of metal complexes at different central metals can be observed from the C═N π* peaks of the ligands, which reflect the metal 3d electronic configurations in the N K-edge XAS spectra. The coordination structures of the metal complexes in solution are discussed based on the XAS spectra of the ligand sides rather than those of the central metal sides. The present analysis method is generally effective for investigating various chemical and biochemical processes such as photosynthetic reactions, biological redox reactions, and artificial photosynthetic reactions, which most metal complexes in solution or protein scaffolds involve. We have confirmed that N K-edge XAS is a powerful technique that enables direct comparison of the electronic structures of metalloporphyrins with their coordination structures in solution or protein scaffolds without using model complexes. Our developed system can obtain the true N K-edge XAS spectra of metalloporphyrins in solution using a transmission measurement. The transmission measurement can be performed with low photon flux of soft X-rays, which is suitable for macromolecules and biological samples with avoiding radiation induced sample damages. We have confirmed that several mM ligands in aqueous solution can be observed in both C and N K-edge XAS. Carbon K-edge XAS can detect the C═N π* peak of several mM ligands in organic solvents that consist of single bonds such as tetrahydrofuran. The liquid cell for XAS needs the small exchange amount less than 1 mL with no limit to sample selection. It means that our measurement system is applicable to precious samples of metalloporphyrins which are difficult to synthesize in large quantities. Recently, we have investigated the photoinduced dynamics of Fe complexes in aqueous solution using time-resolved N K-edge XAS of the ligands.[48] We expect that these developments pave the way for investigating the relaxation processes in the photoreactions of metal complexes in solutions by analyzing the electronic structures of ligands.

Author contributions

Masanari Nagasaka: conceptualization, data curation, formal analysis, funding acquisition, investigation, methodology, project administration, resources, supervision, validation, visualization, writing – original draft, writing – review & editing; Shota Tsuru: data curation, formal analysis, investigation, methodology, resources, validation, visualization, writing – original draft, writing – review & editing; Yasuyuki Yamada: formal analysis, funding acquisition, investigation, supervision, validation, visualization, writing – original draft, writing – review & editing.

Data availability

Data are available from the authors upon reasonable request.

Conflicts of interest

There are no conflicts to declare.

Acknowledgements

This work is supported by JSPS KAKENHI (Grant No. JP19H02680 and JP22H02156). The experiments were performed at the BL3U of UVSOR Synchrotron Facility, Institute for Molecular Science (IMS program no. 19-518 and 20-719). This research is partially funded by the Alexander von Humboldt Foundation through a Research Fellowship to S. T. (JPN1201668 HFST-P). The calculations have benefited from the DTU Computing Center resources.[49]

Open Access Article. Published on 27 August 2024. Downloaded on 5/4/2026 4:07:56 PM. This article is licensed under a Creative Commons Attribution-NonCommercial 3.0 Unported Licence.

References

1 M. Knapp and J. Bridwell-Rabb, *Nat. Chem.*, 2022, **14**, 1202.
2 I. Beletskaya, V. S. Tyurin, A. Y. Tsivadze, R. Guilard and C. Stern, *Chem. Rev.*, 2009, **109**, 1659–1713.
3 W. R. Scheidt and C. A. Reed, *Chem. Rev.*, 1981, **81**, 543–555.
4 J. K. M. Sanders, N. Bampos, Z. Clyde-Watson, S. L. Darling, J. C. Hawley, H.-J. Kim, C. C. Mak and S. J. Webb, in *The Porphyrin Handbook, Inorganic, organometallic and coordination chemistry*, ed. K. M. Kadish, K. M. Smith and R. Guilard, Academic Press, San Diego, CA, 2000, vol. 3, pp. 1–48.
5 L. Cheng and G. B. Richter-Addo, in *The Porphyrin Handbook, Biochemistry and binding: activation of small molecules*, ed. K. M. Kadish, K. M. Smith and R. Guilard, Academic Press, San Diego, CA, 2000, vol. 4, pp. 219–291.
6 M. T. Green, J. H. Dawson and H. B. Gray, *Science*, 2004, **304**, 1653–1656.
7 K. M. Kadish, K. M. Smith and R. Guilard, *The Porphyrin Handbook, Biochemistry and binding: activation of small molecules*, Academic Press, San Diego, CA, vol. 4, 2000.
8 T. E. Westre, P. Kennepohl, J. G. DeWitt, B. Hedman, K. O. Hodgson and E. I. Solomon, *J. Am. Chem. Soc.*, 1997, **119**, 6297–6314.
9 M. L. Baker, M. W. Mara, J. J. Yan, K. O. Hodgson, B. Hedman and E. I. Solomon, *Coord. Chem. Rev.*, 2017, **345**, 182–208.
10 S. A. Wilson, E. Green, I. I. Mathews, M. Benfatto, K. O. Hodgson, B. Hedman and R. Sarangi, *Proc. Natl. Acad. Sci. U. S. A.*, 2013, **110**, 16333–16338.
11 C. Bressler and M. Chergui, *Annu. Rev. Phys. Chem.*, 2010, **61**, 263–282.
12 S. Nozawa, T. Sato, M. Chollet, K. Ichiyanagi, A. Tomita, H. Fujii, S. Adachi and S. Koshihara, *J. Am. Chem. Soc.*, 2010, **132**, 61–63.
13 C. J. Milne, T. J. Penfold and M. Chergui, *Coord. Chem. Rev.*, 2014, **277–278**, 44–68.
14 C. Römelt, J. Song, M. Tarrago, J. A. Rees, M. van Gastel, T. Weyhermüller, S. DeBeer, E. Bill, F. Neese and S. Ye, *Inorg. Chem.*, 2017, **56**, 4745–4750.
15 D. Mendoza, S. Dong, N. Kostopoulos, V. Pinty, O. Rivada-Wheelaghan, E. Anxolabéhère-Mallart, M. Robert and B. Lassalle-Kaiser, *ChemCatChem*, 2023, **15**, e202201298.
16 J. W. Smith and R. J. Saykally, *Chem. Rev.*, 2017, **117**, 13909–13934.
17 K. Atak, R. Golnak, J. Xiao, E. Suljoti, M. Pflüger, T. Brandenburg, B. Winter and E. F. Aziz, *J. Phys. Chem. B*, 2014, **118**, 9938–9943.
18 R. Golnak, J. Xiao, K. Atak, M. Khan, E. Suljoti and E. F. Aziz, *J. Phys. Chem. B*, 2015, **119**, 3058–3062.
19 K. Atak, R. Golnak, J. Xiao, M. Pflüger, T. Brandenburg, B. Winter and E. F. Aziz, *Phys. Chem. Chem. Phys.*, 2015, **17**, 3409–3414.
20 J. Xiao, R. Golnak, K. Atak, M. Pflüger, M. Pohl, E. Suljoti, B. Winter and E. F. Aziz, *J. Phys. Chem. B*, 2014, **118**, 9371–9377.
21 N. A. Schmidt, R. Fink and W. Hieringer, *J. Chem. Phys.*, 2010, **133**, 054703.
22 R. Golnak, J. Xiao, K. Atak, J. S. Stevens, A. Gainar, S. L. M. Schroeder and E. F. Aziz, *Phys. Chem. Chem. Phys.*, 2015, **17**, 29000–29006.
23 M. Fondell, S. Eckert, R. M. Jay, C. Weniger, W. Quevedo, J. Niskanen, B. Kennedy, F. Sorgenfrei, D. Schick, E. Giangrisostomi, R. Ovsyannikov, K. Adamczyk, N. Huse, P. Wernet, R. Mitzner and A. Föhlisch, *Struct. Dyn.*, 2017, **4**, 054902.
24 K. Witte, I. Mantouvalou, R. Sánchez-de-Armas, H. Lokstein, J. Lebendig-Kuhla, A. Jonas, F. Roth, B. Kanngießer and H. Stiel, *J. Phys. Chem. B*, 2018, **122**, 1846–1851.
25 S. S. N. Lalithambika, R. Golnak, B. Winter and K. Atak, *Inorg. Chem.*, 2019, **58**, 4731–4740.
26 R. M. Jay, S. Eckert, R. Mitzner, M. Fondell and A. Föhlisch, *Chem. Phys. Lett.*, 2020, **754**, 137681.
27 R. Büchner, M. Fondell, R. Haverkamp, A. Pietzsch, V. V. da Cruz and A. Föhlisch, *Phys. Chem. Chem. Phys.*, 2021, **23**, 24765–24772.
28 J. M. García-Lastra, P. L. Cook, F. J. Himpsel and A. Rubio, *J. Chem. Phys.*, 2010, **133**, 151103.
29 I. Zegkinoglou, M.-E. Ragoussi, C. D. Pemmaraju, P. S. Johnson, D. F. Pickup, J. E. Ortega, D. Prendergast, G. de la Torre and F. J. Himpsel, *J. Phys. Chem. C*, 2013, **117**, 13357–13364.
30 N. Huse, T. K. Kim, L. Jamula, J. K. McCusker, F. M. F. de Groot and R. W. Schoenlein, *J. Am. Chem. Soc.*, 2010, **132**, 6809–6816.
31 B. E. Van Kuiken, H. Cho, K. Hong, M. Khalil, R. W. Schoenlein, T. K. Kim and N. Huse, *J. Phys. Chem. Lett.*, 2016, **7**, 465–470.
32 R. M. Jay, S. Eckert, B. E. Van Kuiken, M. Ochmann, M. Hantschmann, A. A. Cordones, H. Cho, K. Hong, R. Ma, J. H. Lee, G. L. Dakovski, J. J. Turner, M. P. Minitti, W. Quevedo, A. Pietzsch, M. Beye, T. K. Kim, R. W. Schoenlein, P. Wernet, A. Föhlisch and N. Huse, *J. Phys. Chem. Lett.*, 2021, **12**, 6676–6683.
33 J. D. Koralek, J. B. Kim, P. Brůža, C. B. Curry, Z. Chen, H. A. Bechtel, A. A. Cordones, P. Sperling, S. Toleikis, J. F. Kern, S. P. Moeller, S. H. Glenzer and D. P. DePonte, *Nat. Commun.*, 2018, **9**, 1353.
34 M. Nagasaka, H. Yuzawa and N. Kosugi, *Anal. Sci.*, 2020, **36**, 95–105.
35 M. Nagasaka and N. Kosugi, *Chem. Lett.*, 2021, **50**, 956–964.
36 T. Hatsui, E. Shigemasa and N. Kosugi, *AIP Conf. Proc.*, 2004, **705**, 921–924.
37 M. Nagasaka, H. Yuzawa, T. Horigome and N. Kosugi, *J. Electron Spectrosc. Relat. Phenom.*, 2018, **224**, 93–99.
38 J. Vícha, J. Novotný, M. Straka, M. Repisky, K. Ruud, S. Komorovsky and R. Marek, *Phys. Chem. Chem. Phys.*, 2015, **17**, 24944–24955.
39 T. Yanai, D. P. Tew and N. C. Handy, *Chem. Phys. Lett.*, 2004, **393**, 51–57.
40 E. Epifanovsky, A. T. B. Gilbert, X. Feng, J. Lee, Y. Mao, N. Mardirossian, P. Pokhilko, A. F. White, M. P. Coons, A. L. Dempwolff, Z. Gan, D. Hait, P. R. Horn, L. D. Jacobson, I. Kaliman, J. Kussmann, A. W. Lange, K. U. Lao,

Open Access Article. Published on 27 August 2024. Downloaded on 5/4/2026 4:07:56 PM.
This article is licensed under a Creative Commons Attribution-NonCommercial 3.0 Unported Licence.

D. S. Levine, J. Liu, S. C. McKenzie, A. F. Morrison, K. D. Nanda, F. Plasser, D. R. Rehn, M. L. Vidal, Z.-Q. You, Y. Zhu, B. Alam, B. J. Albrecht, A. Aldossary, E. Alguire, J. H. Andersen, V. Athavale, D. Barton, K. Begam, A. Behn, N. Bellonzi, Y. A. Bernard, E. J. Berquist, H. G. A. Burton, A. Carreras, K. Carter-Fenk, R. Chakraborty, A. D. Chien, K. D. Closser, V. Cofer-Shabica, S. Dasgupta, M. de Wergifosse, J. Deng, M. Diedenhofen, H. Do, S. Ehlert, P.-T. Fang, S. Fatehi, Q. Feng, T. Friedhoff, J. Gayvert, Q. Ge, G. Gidofalvi, M. Goldey, J. Gomes, C. E. González-Espinoza, S. Gulania, A. O. Gunina, M. W. D. Hanson-Heine, P. H. P. Harbach, A. Hauser, M. F. Herbst, M. H. Vera, M. Hodecker, Z. C. Holden, S. Houck, X. Huang, K. Hui, B. C. Huynh, M. Ivanov, Á. Jász, H. Ji, H. Jiang, B. Kaduk, S. Kähler, K. Khistyaev, J. Kim, G. Kis, P. Klunzinger, Z. Koczor-Benda, J. H. Koh, D. Kosenkov, L. Koulias, T. Kowalczyk, C. M. Krauter, K. Kue, A. Kunitsa, T. Kus, I. Ladjánszki, A. Landau, K. V. Lawler, D. Lefrancois, S. Lehtola, R. R. Li, Y.-P. Li, J. Liang, M. Liebenthal, H.-H. Lin, Y.-S. Lin, F. Liu, K.-Y. Liu, M. Loipersberger, A. Luenser, A. Manjanath, P. Manohar, E. Mansoor, S. F. Manzer, S.-P. Mao, A. V. Marenich, T. Markovich, S. Mason, S. A. Maurer, P. F. McLaughlin, M. F. S. J. Menger, J.-M. Mewes, S. A. Mewes, P. Morgante, J. W. Mullinax, K. J. Oosterbaan, G. Paran, A. C. Paul, S. K. Paul, F. Pavošević, Z. Pei, S. Prager, E. I. Proynov, Á. Rák, E. Ramos-Cordoba, B. Rana, A. E. Rask, A. Rettig, R. M. Richard, F. Rob, E. Rossomme, T. Scheele, M. Scheurer, M. Schneider, N. Sergueev, S. M. Sharada, W. Skomorowski, D. W. Small, C. J. Stein, Y.-C. Su, E. J. Sundstrom, Z. Tao, J. Thirman, G. J. Tornai, T. Tsuchimochi, N. M. Tubman, S. P. Veccham, O. Vydrov, J. Wenzel, J. Witte, A. Yamada, K. Yao, S. Yeganeh, S. R. Yost, A. Zech, I. Y. Zhang, X. Zhang, Y. Zhang, D. Zuev, A. Aspuru-Guzik, A. T. Bell, N. A. Besley, K. B. Bravaya, B. R. Brooks, D. Casanova, J.-D. Chai, S. Coriani, C. J. Cramer, G. Cserey, A. E. DePrince, III, R. A. DiStasio, Jr., A. Dreuw, B. D. Dunietz, T. R. Furlani, W. A. Goddard, III, S. Hammes-Schiffer, T. Head-Gordon, W. J. Hehre, C.-P. Hsu, T.-C. Jagau, Y. Jung, A. Klamt, J. Kong, D. S. Lambrecht, W. Liang, N. J. Mayhall, C. W. McCurdy, J. B. Neaton, C. Ochsenfeld, J. A. Parkhill, R. Peverati, V. A. Rassolov, Y. Shao, L. V. Slipchenko, T. Stauch, R. P. Steele, J. E. Subotnik, A. J. W. Thom, A. Tkatchenko, D. G. Truhlar, T. Van Voorhis, T. A. Wesolowski, K. B. Whaley, H. L. Woodcock, III, P. M. Zimmerman, S. Faraji, P. M. W. Gill, M. Head-Gordon, J. M. Herbert and A. I. Krylov, *J. Chem. Phys.*, 2021, **155**, 084801.

41 T. Nakajima, M. Katouda, M. Kamiya and Y. Nakatsuka, *Int. J. Quantum Chem.*, 2015, **115**, 349–359.

42 N. A. Besley, *Acc. Chem. Res.*, 2020, **53**, 1306–1315.

43 C. D. Rankine and T. J. Penfold, *J. Phys. Chem. A*, 2021, **125**, 4276–4293.

44 K. A. de Villiers, C. H. Kaschula, T. J. Egan and H. M. Marques, *J. Biol. Inorg. Chem.*, 2007, **12**, 101–117.

45 B. Johansson and N. Mårtensson, *Phys. Rev. B: Condens. Matter Mater. Phys.*, 1980, **21**, 4427–4457.

46 A. J. Bearden, T. H. Moss, W. S. Caughey and C. A. Beaudreau, *Proc. Natl. Acad. Sci. U. S. A.*, 1965, **53**, 1246–1253.

47 M. Nagasaka, T. Hatsui, H. Setoyama, E. Rühl and N. Kosugi, *J. Electron Spectrosc. Relat. Phenom.*, 2011, **183**, 29–35.

48 F. Kumaki, M. Nagasaka, R. Fukaya, Y. Okano, S. Yamashita, S. Nozawa, S. Adachi and J. Adachi, *J. Chem. Phys.*, 2023, **158**, 104201.

49 DTU Computing Center, *DTU Computing Center resources*, DOI: **10.48714/DTU.HPC.0001**, (accessed August 2024).